Use of Lagrange Multipliers to Combine 1D Variable Kinematic Finite Elements

E. Carrera[ab*], A. Pagani[a†], M. Petrolo[a‡]

[a]Department of Mechanical and Aerospace Engineering, Politecnico di Torino
Corso Duca degli Abruzzi 24, 10129 Torino, Italy.

[b]King Abdulaziz University, Jeddah, Saudi Arabia.

Submitted to:

Computers and Structures

Author for correspondence:
E. Carrera, Professor of Aerospace Structures and Aeroelasticity,
Department of Mechanical and Aerospace Engineering,
Politecnico di Torino,
Corso Duca degli Abruzzi 24,
10129 Torino, Italy,
tel: +39 011 090 6836,
fax: +39 011 090 6899,
e-mail: erasmo.carrera@polito.it

*Professor of Aerospace Structures and Aeroelasticity, e-mail: erasmo.carrera@polito.it
†Ph.D. student, e-mail: alfonso.pagani@polito.it
‡Research Assistant, e-mail: marco.petrolo@polito.it

Abstract

This paper deals with finite element problems that require different formulations in different subregions of the problem domain. Attention is focused on a variable kinematic, one-dimensional, finite element formulation which was recently introduced by the first author. Finite elements with different order of expansion over the cross-section plane are employed in different regions of the 1D domain. Lagrange multipliers are used to "mix" different elements. Constraints are imposed on displacement variables at a number of points whose location over the cross-section is a parameter of the method. The number and the location of the connection points can be modified until convergence is reached. The method is first assessed by encompassing sample problems and then it is applied to analyze a number of structures which requires different formulations in different regions. Compact, thin-walled and bridge-like sections are considered to show the effectiveness of the methodology proposed as well as its advantages to solve practical problems.

Keywords: Global/Local Analysis, Variable Kinematic Models, Lagrange Multipliers, Finite Elements, Refined Beam Theories, Unified Formulation

1 Introduction

In structural engineering, a large amount of applications make use of one- (1D, beam) and two-dimensional (2D, plate/shell) finite elements. For instance, the use of beam elements is of particular interest with slender bodies such as aircraft wings, helicopter rotor blades and bridges. On the other hand, plates and shells are often used when the thickness of the structure is negligible if compared to the other two dimensions. 1D and 2D finite elements provide computationally efficient and easy-to-construct models. Nevertheless, structures may contain regions where three-dimensional (3D) stress fields occur. To accurately capture these localized 3D stress fields, solid models or higher-order theories are necessary. However, in order to make the model more efficient, a global/local approach is usually employed. Two main approaches are available to deal with a global/local analysis: (1) refining the mesh or the shape functions in correspondence with the critical domain [1, 2, 3, 4, 5]; (2) formulating multi model methods, in which different subregions of the structure are analysed with different mathematical models [6, 7, 8, 9, 10, 11, 12, 13].

To couple coarse and refined subregions of a structure, adaptive techniques are often used. The *h*-adaption method [1] is used when the structure's subregions differ in mesh size, whereas the *p*-adaption method [2] can be applied when the subregions differ in the polynomial order of the shape functions. Moreover, the *hp*-adaption [3] can allow the implementation of subregions differing in both mesh size and shape functions. Other techniques allowing for the coupling of different meshes are, for instance, the multi-grid method [4], the extended finite element method (XFEM) [5], and the mortar method [14]. The methods mentioned so far can be addressed as single-model methods. In the case of multiple-model methods, where different subregions of the structure are modeled with kinematically incompatible elements, the compatibility of displacements and equilibrium of stresses at the interface between dissimilar elements have to be achieved. In the *s*-version of the finite element method (FEM) [6, 7], the resolution in a certain subregion of the structure is increased by superimposing additional meshes of higher-order hierarchical elements. In [8], Shim at al. combined 1D and 2D finite elements with 3D solid elements via multipoint constraint equations evaluated by equating the work done on either side of the dimensional interface. In [9], the coupling of structural models with different dimensionality was achieved by exploiting conditions derived from the governing variational principle formulated at the continuous level. In the global/local method proposed by Mao et al. in [10], a coarse mesh was used to analyse the entire structure to obtain the nodal displacements which were subsequently used as displacement boundary conditions for the refined regions of interest. Ben Dhia [11] proposed the Arlequin method to couple different numerical models. This method was adopted by Hu et al. [12] for the linear analysis of sandwich beams modelled via 1D and 2D finite elements. In recent works [13, 15], the Arlequin method was formulated in the context of the Carrera Unified Formulation (CUF) to couple 1D finite elements differing in the approximation order of the displacement field.

This work presents variable kinematic elements based on 1D CUF models and Taylor expansions of the displacement field. Over the years, improvements in classical 1D models (Euler-Bernoulli, hereafter referred

to as EBBM, and Timoshenko, hereafter referred to as TBM) have been proposed to account for non-classical effects and non-conventional materials. A general review on beam modelling was proposed by Kapania and Raciti [16, 17] accounting for static, buckling, free-vibration and wave propagation analysis. Other reviews are those by Hodges [18] and Jung et al. [19]. CUF for 1D theories was recently proposed by the first author and his co-workers [20, 21]. In the present paper, Taylor-expansion- (TE) based 1D CUF models are used to formulate variable kinematic 1D elements. TE models exploit Taylor-like polynomials of order N to define the displacement field above the cross-section, with N as a free parameter of the formulation. In static [22, 23] and free-vibration analysis [24, 25], the strength of CUF TE models in dealing with arbitrary geometries, thin-walled structures and local effects was evident. Moreover, an asymptotic-like analysis aimed at reducing refined models were carried out in [26]. EBBM and TBM classical beam theories can be derived from the linear ($N = 1$) Taylor-type expansion. In this work, the coupling between different order TE elements is achieved with the method of the Lagrange multipliers. Lagrange multipliers are widely used in computational mechanics. The book by Zienkiewicz and Taylor [27] shows the use of multipliers for contact and tied interfaces, for multibody coupling (in particular, to connect a rigid body to a flexible body or simply to have two or more rigid bodies connected in some specific manner), and to avoid the necessity of C^1 continuity for the problem of thin plates.

In the next section a brief overview on CUF is provided. Subsequently, the method of the Lagrange multipliers is extended in the context of the unified formulation. Next, numerical results concerning the use of multipliers to apply cross-sectional and localized boundary conditions are presented. Two examples of 1D variable kinematic models are then addressed. Finally, the main conclusions are outlined.

2 Variable Kinematic 1D Models based on the Unified Formulation

The adopted coordinate frame is presented in Fig. 1. Let us introduce the transposed displacement vector,

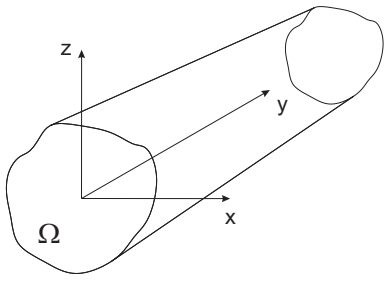

Figure 1: Coordinate frame of the beam model

$$\mathbf{u}(x,y,z) = \left\{ \begin{array}{ccc} u_x & u_y & u_z \end{array} \right\}^T \tag{1}$$

The cross-section of the structure is denoted by Ω, and the beam boundaries over y are $0 \leq y \leq L$. The stress, $\boldsymbol{\sigma}$, and strain, $\boldsymbol{\epsilon}$, components are grouped as follows:

$$\begin{aligned} \boldsymbol{\sigma}_p &= \left\{ \begin{array}{ccc} \sigma_{zz} & \sigma_{xx} & \sigma_{zx} \end{array} \right\}^T, \quad \boldsymbol{\epsilon}_p = \left\{ \begin{array}{ccc} \epsilon_{zz} & \epsilon_{xx} & \epsilon_{zx} \end{array} \right\}^T \\ \boldsymbol{\sigma}_n &= \left\{ \begin{array}{ccc} \sigma_{zy} & \sigma_{xy} & \sigma_{yy} \end{array} \right\}^T, \quad \boldsymbol{\epsilon}_n = \left\{ \begin{array}{ccc} \epsilon_{zy} & \epsilon_{xy} & \epsilon_{yy} \end{array} \right\}^T \end{aligned} \tag{2}$$

The subscript "n" stands for terms lying on the cross-section, while "p" stands for terms lying on planes which are orthogonal to Ω. In the case of small displacements with respect to a characteristic dimension of Ω, the strain - displacement relations are

$$\begin{aligned} \boldsymbol{\epsilon}_p &= \boldsymbol{D}_p \mathbf{u} \\ \boldsymbol{\epsilon}_n &= \boldsymbol{D}_n \mathbf{u} = (\boldsymbol{D}_{n\Omega} + \boldsymbol{D}_{ny}) \mathbf{u} \end{aligned} \tag{3}$$

where $\boldsymbol{D}_p$ and $\boldsymbol{D}_n$ are linear differential operators and they are not reported here. They can be found in [20]. Constitutive laws are exploited to obtain stress components,

$$\boldsymbol{\sigma} = \boldsymbol{C} \boldsymbol{\epsilon} \tag{4}$$

According to Eq.n (2), the previous equation becomes

$$\begin{aligned} \boldsymbol{\sigma}_p &= \tilde{\boldsymbol{C}}_{pp} \boldsymbol{\epsilon}_p + \tilde{\boldsymbol{C}}_{pn} \boldsymbol{\epsilon}_n \\ \boldsymbol{\sigma}_n &= \tilde{\boldsymbol{C}}_{np} \boldsymbol{\epsilon}_p + \tilde{\boldsymbol{C}}_{nn} \boldsymbol{\epsilon}_n \end{aligned} \tag{5}$$

The matrices $\tilde{\boldsymbol{C}}_{pp}$, $\tilde{\boldsymbol{C}}_{nn}$, $\tilde{\boldsymbol{C}}_{pn}$, and $\tilde{\boldsymbol{C}}_{np}$ contains the material coefficients and they can be found in [20]. For the sake of brevity, the dependence of material coefficients versus Young's modulus and Poisson's ratio are not reported here. The reader is referred to [28, 29] for further details.

In the framework of the CUF, the displacement field above the cross-section is the expansion of generic functions, F_τ,

$$\mathbf{u}(x, y, z) = F_\tau(x, z) \mathbf{u}_\tau(y), \qquad \tau = 1, 2, ..., M \tag{6}$$

where F_τ vary over the cross-section. $\mathbf{u}_\tau$ is the generalized displacement vector and M stands for the number of terms of the expansion. According to the generalized Einstein notation, the repeated subscript, τ, indicates summation. The choice of F_τ determines the class of the 1D CUF model that has to be adopted. The Taylor-expansion 1D models are based on polynomial expansions, $x^i \ z^j$, of the displacement field above the cross-section of the structure, where i and j are positive integers. For instance, the displacement field of the

second-order TE model (TE2) is expressed by

$$\begin{aligned} u_x &= u_{x_1} + x\ u_{x_2} + z\ u_{x_3} + x^2\ u_{x_4} + xz\ u_{x_5} + z^2\ u_{x_6} \\ u_y &= u_{y_1} + x\ u_{y_2} + z\ u_{y_3} + x^2\ u_{y_4} + xz\ u_{y_5} + z^2\ u_{y_6} \\ u_z &= u_{z_1} + x\ u_{z_2} + z\ u_{z_3} + x^2\ u_{z_4} + xz\ u_{z_5} + z^2\ u_{z_6} \end{aligned} \tag{7}$$

The order of the expansion is arbitrary and it can be set as an input of the analysis.

In order to discretize the structure along the y-axis, the FEM is adopted. This process is conducted via a classical finite element technique, where the displacement vector is given by

$$\mathbf{u}(x, y, z) = F_\tau(x, z) N_i(y) \mathbf{q}_{\tau i} \tag{8}$$

where N_i stands for the shape functions and $\mathbf{q}_{\tau i}$ for the nodal unknowns,

$$\mathbf{q}_{\tau i} = \left\{ \begin{array}{ccc} q_{u_{x_{\tau i}}} & q_{u_{y_{\tau i}}} & q_{u_{z_{\tau i}}} \end{array} \right\}^T \tag{9}$$

For the sake of brevity, the shape functions are not reported here. They can be found in many books, for instance in [3]. Elements with four nodes (B4) are adopted in this work, that is, a cubic approximation along the y-axis is assumed. The choice of the theory order is completely independent of the choice of the beam finite element to be used along the axis of the beam.

The stiffness matrix of the elements and the vector of external loadings are obtained via the principle of virtual displacement

$$\delta L_{int} = \int_V (\delta \boldsymbol{\epsilon}_p^T \boldsymbol{\sigma}_p + \delta \boldsymbol{\epsilon}_n^T \boldsymbol{\sigma}_n) dV = \delta L_{ext} \tag{10}$$

where L_{int} stands for the strain energy, L_{ext} is the work of the external loadings and δ stands for the virtual variation. The virtual variation of the strain energy was rewritten using Eq.n (3), (5) and (8):

$$\delta L_{int} = \delta \mathbf{q}_{\tau i}^T \mathbf{K}^{ij\tau s} \mathbf{q}_{sj} \tag{11}$$

where $\mathbf{K}^{ij\tau s}$ is the stiffness matrix in the form of the fundamental nucleus. In a compact notation, it can be written as:

$$\begin{aligned} \boldsymbol{K}^{ij\,\tau s} \;=\; & I_l^{\,ij} \triangleleft \left(\boldsymbol{D}_{np}^T\, F_\tau\, \boldsymbol{I}\right) \Big[\tilde{\boldsymbol{C}}_{np} \left(\boldsymbol{D}_p\, F_s\, \boldsymbol{I}\right) \;+\; \tilde{\boldsymbol{C}}_{nn} \left(\boldsymbol{D}_{np}\, F_s\, \boldsymbol{I}\right) \Big] \;+ \\ & \left(\boldsymbol{D}_p^T\, F_\tau\, \boldsymbol{I}\right) \Big[\tilde{\boldsymbol{C}}_{pp} \left(\boldsymbol{D}_p\, F_s\, \boldsymbol{I}\right) \;+\; \tilde{\boldsymbol{C}}_{pn} \left(\boldsymbol{D}_{np}\, F_s\, \boldsymbol{I}\right) \Big] \triangleright_\Omega \;+ \\ & I_l^{\,ij,_y} \triangleleft \Big[\left(\boldsymbol{D}_{np}^T\, F_\tau\, \boldsymbol{I}\right) \tilde{\boldsymbol{C}}_{nn} \;+\; \left(\boldsymbol{D}_p^T\, F_\tau\, \boldsymbol{I}\right) \tilde{\boldsymbol{C}}_{pn} \Big] F_s \triangleright_\Omega \boldsymbol{I}_{\Omega\, y} \;+ \\ & I_l^{\,i,_y j}\, \boldsymbol{I}_{\Omega\, y} \triangleleft F_\tau \Big[\tilde{\boldsymbol{C}}_{np} \left(\boldsymbol{D}_p\, F_s\, \boldsymbol{I}\right) \;+\; \tilde{\boldsymbol{C}}_{nn} \left(\boldsymbol{D}_{np}\, F_s\, \boldsymbol{I}\right) \Big] \triangleright_\Omega \;+ \\ & I_l^{\,i,_y j,_y}\, \boldsymbol{I}_{\Omega\, y} \triangleleft F_\tau\, \tilde{\boldsymbol{C}}_{nn}\, F_s \triangleright_\Omega \boldsymbol{I}_{\Omega\, y} \end{aligned} \tag{12}$$

where

$$\boldsymbol{I}_{\Omega\, y} = \begin{bmatrix} 0 & 1 & 0 \\ 1 & 0 & 0 \\ 0 & 0 & 1 \end{bmatrix} \qquad \triangleleft \ldots \triangleright_{\Omega} = \int_{\Omega} \ldots \, d\Omega \tag{13}$$

$$\left(I_l^{\ ij}, I_l^{ij,_y}, I_l^{i,_y j}, I_l^{i,_y j,_y} \right) = \int_l \left(N_i \, N_j, \, N_i \, N_{j,_y}, \, N_{i,_y} \, N_j, \, N_{i,_y} \, N_{j,_y} \right) dy \tag{14}$$

It should be noted that $\mathbf{K}^{ij\tau s}$ does not depend on the expansion order. This is the key-point of CUF which allows, with only nine FORTRAN statements, the implementation of any-order of multiple class theories. The loadings vector which is variationally coherent to the model in not derived here, it can be found in [20].

3 Combining Variable Kinematic Models via Lagrange Multipliers

The method of Lagrange multipliers provides the stationary conditions of a constrained functional. The calculation of the stationary conditions of a functional with n variables and k boundary conditions is reduced to a stationary points problem of an unconstrained functional of $n + k$ variables. The application of the multipliers to the CUF is provided in this section. A more generic discussion on the multipliers method can be found in [30, 31].

The solution of the problem described in Eq.n (10) is found by calculating the nodal unknowns, $\mathbf{q}$ (see Eq.n (9)), from the following linear system:

$$\boldsymbol{K}\mathbf{q} = \mathbf{F} \tag{15}$$

where $\boldsymbol{K}$ is the stiffness matrix and $\mathbf{F}$ is the loading vector.

The method of the Lagrange multipliers is a well-known technique and it is generally used in FEM when multiple-points constraints have to be imposed. In this work, inter alia, Lagrange multipliers were used for the impositions of localized constraints and displacements on higher-order beam models. However, one of the most important features of the multipliers method is that it allows the imposition of a generic relation between the displacements of two (or more) arbitrary points. By exploiting this feature, we are able to implement variable kinematic models. Let two bodies share a common face. We want to impose the following condition:

$$\mathbf{u}^1(x_k, y_k, z_k) - \mathbf{u}^2(x_k, y_k, z_k) = 0 \tag{16}$$

where $\mathbf{u}^1(x_k, y_k, z_k)$ is the displacement of a point on the interface cross-section of the first body, whereas $\mathbf{u}^2(x_k, y_k, z_k)$ is the displacement of the same point on the interface cross-section of the second body. To impose the above condition, the *Lagrangian* that has to be added to the original system is

$$\Pi = \boldsymbol{\lambda}^T \left(\mathbf{u}^1(x_k, y_k, z_k) - \mathbf{u}^2(x_k, y_k, z_k) \right) \tag{17}$$

where $\boldsymbol{\lambda} = \left\{ \begin{array}{ccc} \lambda_x & \lambda_y & \lambda_z \end{array} \right\}^T$ is the vector containing the Lagrange multipliers. Equation (17) can be rewritten in terms of CUF

$$\Pi = \boldsymbol{\lambda}^T \boldsymbol{B} \mathbf{q} \tag{18}$$

where the fundamental nucleus of the matrix $\boldsymbol{B}$ is

$$\boldsymbol{B}^{\tau i} = \Big(F_\tau^1(x_k, z_k) N_i^1(y_k) - F_\tau^2(x_k, z_k) N_i^2(y_k) \Big) \boldsymbol{I} \tag{19}$$

$\boldsymbol{I}$ is the identity matrix with dimensions 3×3. The superscripts "1" and "2" also denote the fact that, generally, the bodies that are coupled can be modeled with different order theories and with different beam elements along the beam axis.

The solution of the problem is given by finding $\mathbf{q}$ and $\boldsymbol{\lambda}$ from the following linear system:

$$\left\{ \begin{array}{lcl} \boldsymbol{K}\mathbf{q} + \dfrac{\partial \Pi}{\partial \mathbf{q}} & = & \mathbf{F} \\ \dfrac{\partial \Pi}{\partial \boldsymbol{\lambda}} & = & \overline{\mathbf{u}} \end{array} \right. \tag{20}$$

where $\overline{\mathbf{u}}$ is zero in the case of the homogeneous condition given in Eq.n (16). Equation (20) can be rewritten using Eq.n (18). In a matrix form it reads

$$\begin{bmatrix} \boldsymbol{K} & \boldsymbol{B}^T \\ \boldsymbol{B} & 0 \end{bmatrix} \begin{bmatrix} \mathbf{q} \\ \boldsymbol{\lambda} \end{bmatrix} = \begin{bmatrix} \boldsymbol{F} \\ 0 \end{bmatrix} \tag{21}$$

Beam elements based on different kinematic models are connected by imposing the condition described above on a certain number of points - *connection points* - on the interface cross-section. The use of the multipliers method offers many advantages. However, the main disadvantage of its use in structural problems is that the matrix of Eq.n (21) is not, in general, positive definite.

4 Numerical Results

Several structural problems were considered. The first part of this section concerns the use of the method of the Lagrange multipliers to apply arbitrary geometrical conditions on higher-order beam models. In particular, the possibility of dealing with localized constraints is shown. Afterwards, attention is focused on the imposition of displacements at arbitrary points of the structure. The second part of this section deals with variable kinematic models. Higher-order models were obtained by means of the CUF, whereas the multipliers method was used to impose compatibility of displacements at points on the interface cross-section between different order beam elements. First, the results from variable kinematics models of a compact square beam are proposed. Subsequently, a thin-walled cylinder and a bridge-like structure are proposed. The results are

compared to those from the literature and to solutions given by a commercial FEM code.

4.1 Lagrange multipliers to impose localized constraints and displacements

One of the most important feature of the method of the Lagrange multipliers used for refined beam models is that boundary conditions can be effective and applied at points not lying on the beam axis. This could be the case of many practical problems.

To show the effectiveness of multipliers in dealing with localized constraints, a compact square beam was considered in Example 1. The length of the beam, L, was set to 2 m. The cross-section was a square with sides, a, equal to 0.2 m. The structure was made of isotropic material with Young's modulus $E = 75$ GPa and Poisson's ratio $\nu = 0.33$. A compression load, $F_y = -50 \times 10^3$ N, was applied at $(0, L, 0)$. The beam had four clamped constraints ($u_x = u_y = u_z = 0$) in four different points, as shown in Fig. 2. Table 1 shows the

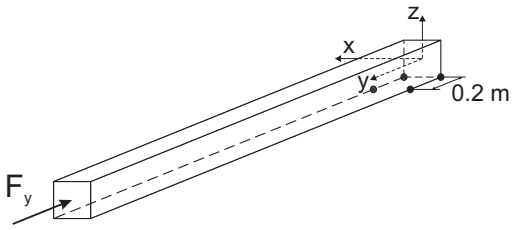

Figure 2: Example 1. Localized clamped constraints, compact square beam undergoing a compressive load

axial, u_y, and vertical displacement, u_z, at the loaded point for different refined TE models constructed with 10 B4 elements. Figure 3 shows the deformed configuration of the fourth-order TE model. If the beam had

	TE1	TE2	TE3	TE4
$-u_y \times 10^4$ $[m]$	0.351	0.390	0.471	0.558
$u_z \times 10^3$ $[m]$	0.093	0.152	0.251	0.344

Table 1: Axial (u_y) and vertical (u_z) displacements at the loaded point of the locally constrained beam of Example 1

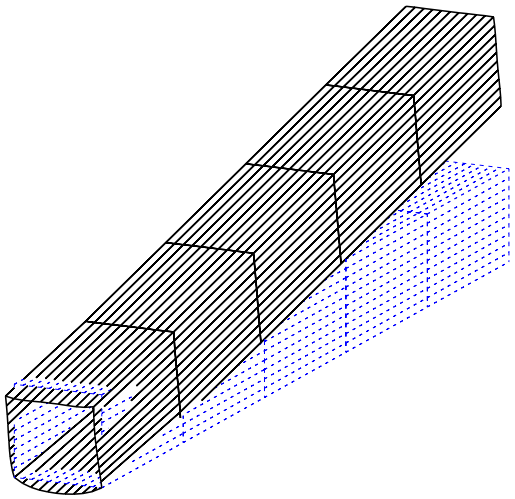

Figure 3: Un-deformed and deformed configuration of the asymmetrically constrained beam of Example 1

been constrained in a symmetrical manner, the structure would have been subjected to a pure compression state. Because of the asymmetric locations of the constrains, the beam is subjected to bending as well as compression.

As second assessment of the use of multipliers to apply arbitrary boundary conditions, the compact square beam of the previous example has again been considered in Example 2. The whole cross-section was clamped at $y = 0$ and two axial displacements, $\overline{u}_y$, were imposed at the free end, as shown in Fig. 4. Two cases are

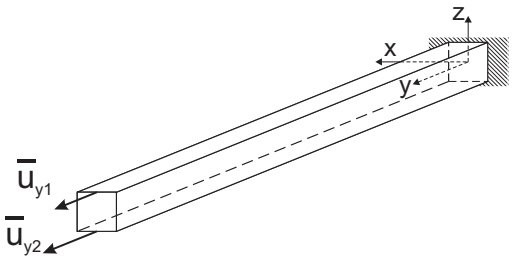

Figure 4: Example 2. Imposed displacements on the cantilever beam

addressed in Example 2, differing in the choice of the imposed displacement $\overline{u}_y$ (see Eq.n (20)):

Case 1: $\overline{u}_{y_1} = -\overline{u}_{y_2} = 1$ mm

Case 2: $\overline{u}_{y_1} = 5$ mm, $\overline{u}_{y_2} = -1$ mm

At the same points where axial displacements are imposed, x- and z-wise displacement components were left free. The distributions of the axial stress, σ_{yy}, at $x = y = 0$ for the linear (TE1), the quadratic (TE2) and the cubic (TE3) TE model are shown in Fig. 5. Figure 6 and Fig. 7 show the values of the Lagrange

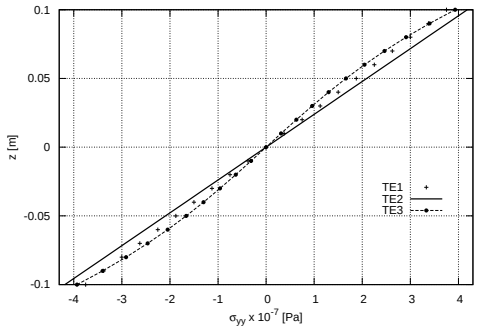

(a) Case 1

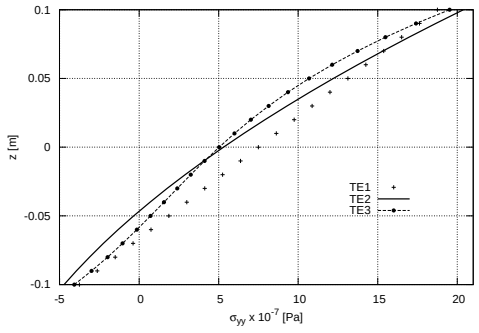

(b) Case 2

Figure 5: Example 2. Axial stress, σ_{yy}, versus the z-axis, beam subjected to imposed displacements

multipliers for *Case 1* and *Case 2*, respectively. Value k takes on values from 1 to $DOFs\_cn + 2$, where $k = 1, ..., DOFs\_cn$ represent the degrees of freedom at the clamped end, whereas the degrees of freedom associated to $k = DOFs\_cn + 1$ and $k = DOFs\_cn + 2$ are those added by the multipliers method to impose the two displacements at the free end. The following statements hold.

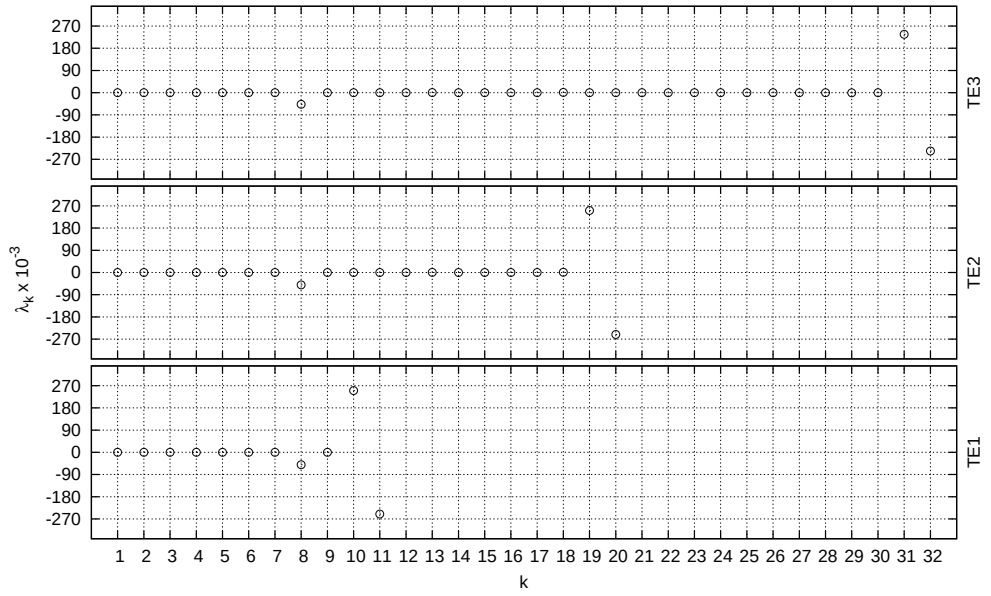

Figure 6: Example 2. Values of the Lagrange multipliers, *Case 1* of the beam subjected to imposed displacements

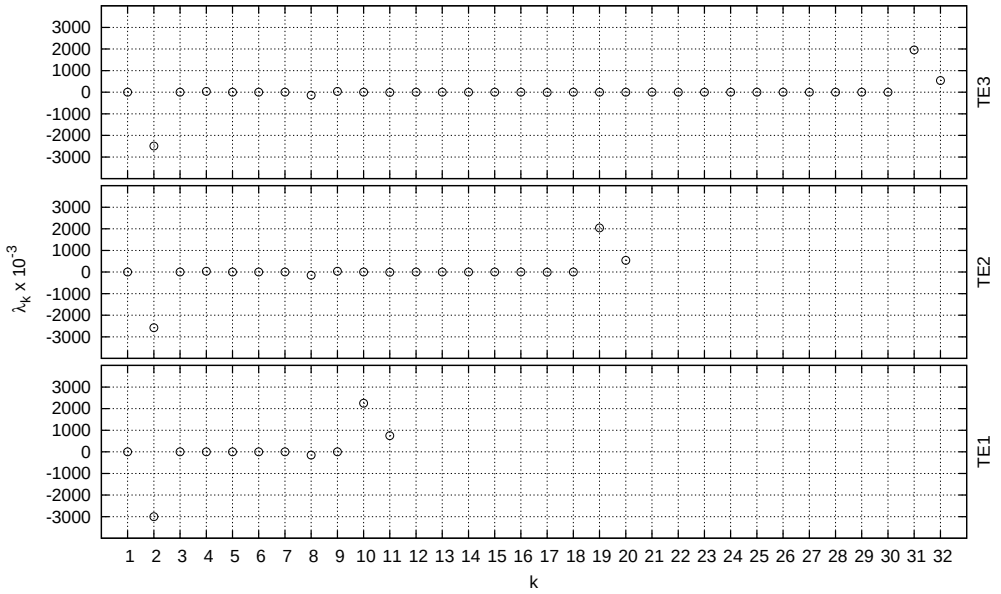

Figure 7: Example 2. Values of the Lagrange multipliers, *Case 2* of the beam subjected to imposed displacements

1. The Lagrange multipliers placed in correspondence with the degrees of freedom whose displacements are imposed, are the forces that have to be applied in order to obtain the displacements themselves.

2. As far as *Case 1* is considered, the only non-zero multiplier in correspondence of the clamp is λ_8, which is the term that concerns the bending moment. The beam has pure bending strain-stress field.

3. In *Case 2* the beam has a bending-traction stain-stress field. In fact, both λ_2 (the term concerning the normal force at the clamped node) and λ_8 are different from zero.

It is concluded that

1. The present method is effective to impose both homogeneous and non-homogeneous geometrical boundary conditions on higher-order beam theories.

2. The method of Lagrange multipliers preserves its effectiveness in the case of variable kinematic 1D finite elements.

4.2 Variable Kinematic Model for Compact Structures

The following example was addressed in the work by Biscani et al. [13], where 1D variable kinematic models based on CUF were obtained exploiting the Arlequin method. The geometrical characteristics were the same as in the previous examples. The material data were set as follows: Young's modulus $E = 75$ GPa and Poisson's ratio $\nu = 0.3$. The beam was simply supported and it underwent a localised uniform pressure, P, equal to 1 Pa acting on 10% of the length and centred at mid-span. Due to the symmetry of the problem, only half of the structure was investigated. Results were computed considering 20 B4 elements of the same length. The loading was applied at the top of the cross-section, as shown in Fig. 8. The cross-section and the

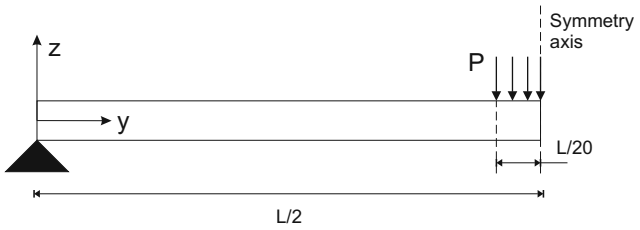

Figure 8: Simply supported beam under a localised uniform pressure P

load are shown in Fig. 9, together with the location of the verification points. Out-of-plane displacement, u_y,

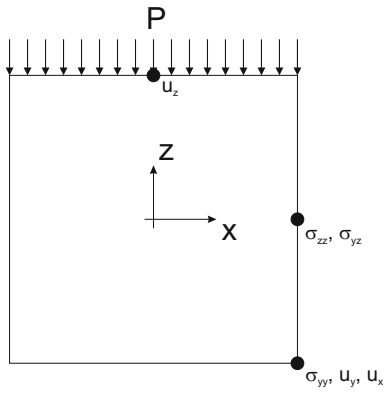

Figure 9: Square cross-section geometry, load and verification points

and shear stress component, σ_{yz}, are evaluated at $y = 0$, whereas in-plane displacement components, u_z and u_x, and normal stresses, σ_{yy} and σ_{zz}, are evaluated at beam mid-span. The results are put in the following

non-dimensional form:

$$(u_x^*, u_y^*, u_z^*) = \frac{Ea}{L^2 P}(u_x, u_y, u_z)$$
$$(\sigma_{yy}^*, \sigma_{yz}^*, \sigma_{zz}^*) = \frac{1}{P}(\sigma_{yy}, \sigma_{yz}, \sigma_{zz}) \tag{22}$$

Table 2 shows the displacements and the stress components obtained with both single model methods and variable kinematic models. First, attention is focused on the classical (EBBM, TBM) and single-theory TE

	$-10^2 \times u_x^*$	$-10^1 \times u_y^*$	u_z^*	$10^{-1} \times \sigma_{yy}^*$	$-10^1 \times \sigma_{yz}^*$	$-10^1 \times \sigma_{zz}^*$	DOFs
EBBM	0	3.736	2.486	1.419	-	-	183
TBM	0	3.736	2.548	1.419	5.000	-	305
TE1	−0.080	3.736	2.548	1.419	5.000	4.395	549
TE2	2.108	3.729	2.532	1.409	5.865	4.265	1098
TE3	2.092	3.735	2.542	1.425	8.462	6.063	1830
TE4	2.116	3.735	2.542	1.423	8.511	6.003	2745
LM^a	2.116	3.699	2.524	1.420	5.000	6.001	1134
LM^b	−0.080	3.732	2.550	1.419	8.429	4.395	1134
Arlequin^a [13]	2.116	3.729	2.537	1.424	5.000	5.217	1197
Arlequin^b [13]	−0.056	3.716	2.547	1.444	8.352	4.807	1197
SOLID	2.123	3.728	2.551	1.426	8.528	6.023	133119

Table 2: Non-dimensional displacements and stresses for the square beam

models up to the fourth-order. The results are validated with a MSC/NASTRAN® model built with solid finite elements. The following considerations arise from the analyses:

1. Bending stress-strain field is predominant. Classical models, therefore, yield accurate results for u_y and u_z. In order to correctly predict u_x, a second-order theory is required.

2. Classical theories correctly predict only σ_{yy}. An accurate evaluation of σ_{yz} and σ_{zz} calls for at least a third-order theory.

As far as variable kinematic models are concerned, two configurations are considered. In the first one, hereafter referred to as the LM^a model, the refined beam elements are placed near the loading application area. In the second configuration, hereafter referred to as the LM^b model, the refined elements are placed near the constraint (see Fig. 10). In particular, for both the LM^a and LM^b models, the coarse sub-domain of the beam

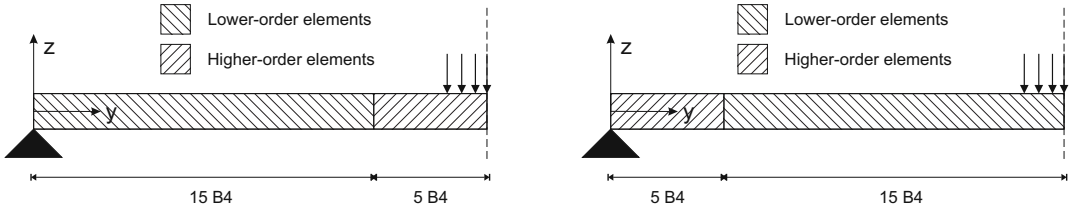

(a) LM^a model (b) LM^b model

Figure 10: Variable kinematic models with refined elements near (a) the loading application zone or (b) the constraint

is modeled with 15 first-order (TE1) B4 elements, whereas the higher-order area of the beam is modeled with

five fourth-order (TE4) B4 elements.

As mentioned in Section 3, the variable kinematic models are obtained by imposing the compatibility of displacement components at a number of points lying on the interface cross-section between two different-order beam elements. The placement and the definition of the minimum number of connection points that have to be used to couple two differently interpolated displacement fields versus accuracy is a key-issue. On this respect, mathematical techniques could be used to choose the set of points. However, the mathematical algorithms developed for regular sample sections wouldn't be convenient in general or difficult to be used for complex and thin-walled geometries. For this reason, in the present paper, the set of connection points is chosen on the basis of a study of the convergence rate of the solution. Therefore, as far as LM^a and LM^b models are concerned, first the convergence of the solution as the number of the connection points increases has to be ensured. A number of cases differing in the number of constrained points on the interface cross-section between the TE1 and the TE4 elements were considered, as shown in Fig. 11. Figure 12 and Table 3

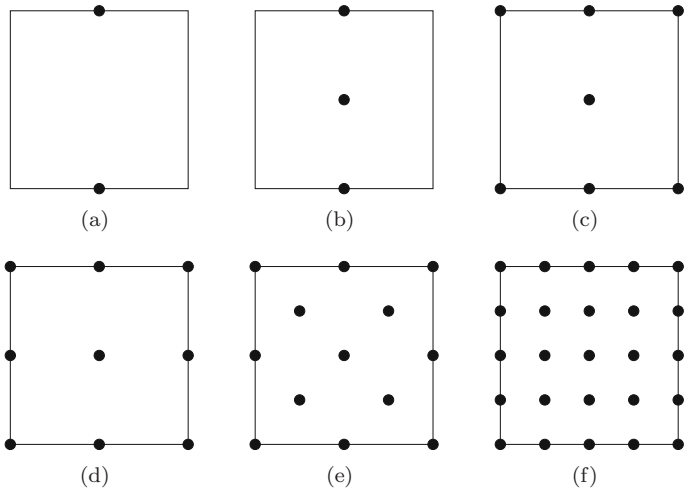

Figure 11: Connection points on the interface cross-section of the variable kinematic models

show the convergence rate of the dimensionless vertical displacement, u_z^*, for both LM^a and LM^b models. It

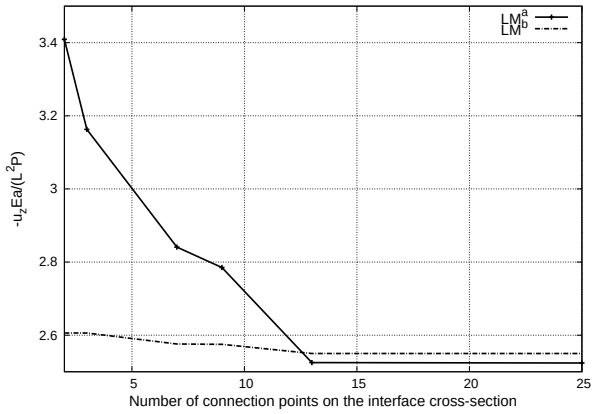

Figure 12: Dimensionless vertical displacement, u_z^*, versus number of constrained points on the interface cross-section

Conn. points	u_z^*	
	LM^a	LM^b
2	3.409	2.606
3	3.163	2.606
7	2.841	2.576
9	2.785	2.575
13	2.525	2.550
25	2.524	2.550

Table 3: Vertical displacement versus the number of connection points, square beam

should be underlined that

1. 13 properly chosen connection points are enough to provide the convergence of the solution for the problem addressed.

2. The choice of the connection points on the interface cross-section depends on the order of the coupled beam elements, the geometry of the structure, the loading condition and the constraints.

The results from the LM^a and the LM^b models are shown in Table 2. The results are compared to those from the solid model, the single higher-order TE models, and variable kinematic models obtained by means of the application of the Arlequin method to 1D CUF. In particular, the models that are addressed as Arlequin^a and Arlequin^b were obtained by Biscani et al. [13] similarly to the LM^a and the LM^b models. In the Arlequin^a model, the refined sub-domain, which is near the loading application area, is modeled with five TE4 elements, whereas the coarse sub-domain is built with 16 TE1 elements. Conversely, in the Arlequin^b model, the refined sub-domain is near the constraint. The main difference between the Arlequin-based and the Lagrange multipliers-based variable kinematic models is that the former include an overlapping region, where a TE1 element coexists with a TE4 element. In the overlapping volume, two solutions exist. Their values do not necessarily match. The following points should be noted:

1. Variable kinematic models provide good results if compared to single model methods and solid models.

2. Both the method of the Lagrange multipliers and the Arlequin methods are effective in building variable kinematic models.

3. A comparison between the variable kinematic models considered and the fourth-order single-model shows that the total number of degrees of freedom is reduced by more than half.

4.3 Variable Kinematic Model for Thin-walled Structures

A thin-walled cylinder was considered. The outer diameter of the cylinder was set to $d = 2$ m, whereas the inner diameter was 1.96 m. The span-to-diameter ratio, L/d, was 10. The material constituting the structure was characterized by Young's modulus, E, equal to 75 GPa and Poisson's ratio $\nu = 0.33$. The cross-section geometry is shown in Fig. 13 together with the loading condition. The cylinder was clamped at $y = 0$ and

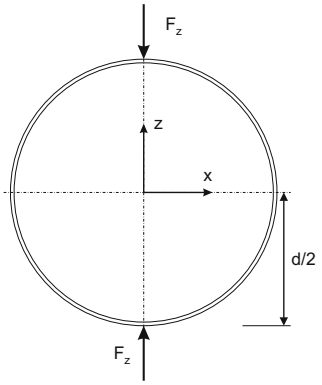

Figure 13: Cross-section of the thin-walled cylinder and loading condition

loaded at $y = L$. The point load, F_z, was equal to 10 kN. The refined 1D models were built with 20 B4 elements of the same length.

First, TE single models are considered. Table 4 shows the vertical displacement, u_z, of the top loaded point, together with the number of the degrees of freedom. The solutions from the classical theories (EBBM, TBM) are not reported, since they do not provide cross-sectional deformations as well as the linear TE1 model. The results are compared to a MSC/NASTRAN® model built with shell finite elements. Figure 14 shows the deformed configuration of the free end of the cylinder for both the TE models and the SHELL model. It is clear that an eleventh-order (TE11) model is necessary to obtain a reliable solution.

	$-u_z$ $[mm]$	DOFs
$TE1$	0	549
$TE3$	0.67	1830
$TE5$	3.56	3843
$TE7$	5.54	6588
$TE9$	6.00	10065
$TE11$	6.23	14274
SHELL	6.62	60000

Table 4: Vertical displacement of the top loaded point, u_z, and number of the degrees of freedom. Pinched cylinder

Variable kinematic models are implemented through Lagrange multipliers to reduce the computational effort of the TE11 model. In particular, since the displacement field involves only the area of the structure which is located in close proximity of the concentrated loads, lower-order TE models can be used where an eleventh-order model is not necessary. The variable kinematic models are obtained considering a lower-order expansion on the first half of the structure (10 B4 elements), whereas a eleventh-order TE is considered in the second half of the cylinder where the loads are applied. Firstly a convergence study is carried out to ensure the independence of the solution from the number of the connection points on the interface cross-section between the lower- and higher-order beam elements. The convergence study is performed considering the TE1/11 variable kinematic model, which is obtained combining 10 TE1 and 10 TE11 B4 elements. Figure 15 and Table 5 show the convergence rate of the vertical displacement of the top loaded point. Figure 16 shows

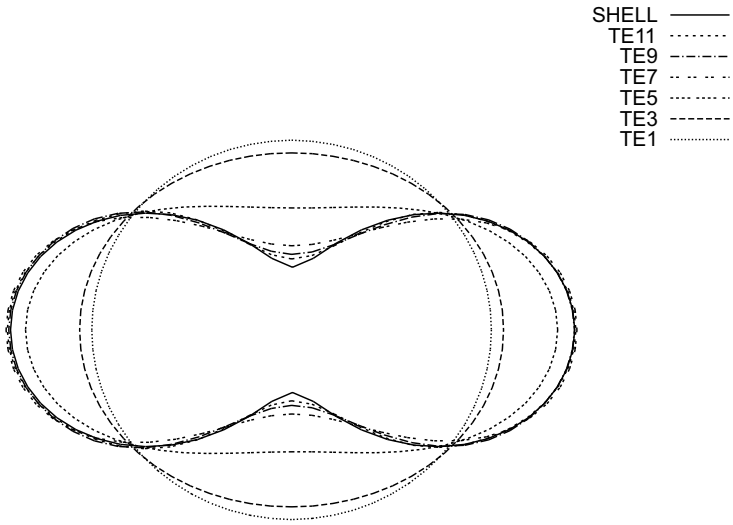

Figure 14: Deformed tip cross-section of the cylinder. Constant-order TE models versus SHELL model

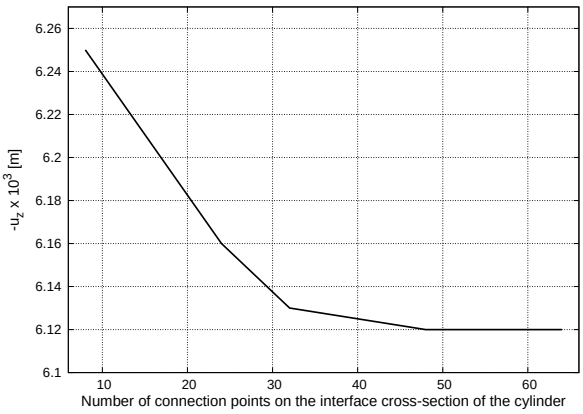

Figure 15: Vertical displacement of the top loaded point, u_z, versus the number of the connection points

Conn. points	$-u_z$ $[mm]$
8	6.25
24	6.16
32	6.13
48	6.12
64	6.12

Table 5: Vertical displacement versus the number of connection points. Pinched cylinder

the considered configurations of the cylinder differing on the location of the connection points on the interface cross-section. It is clear that 48 connection points are enough to ensure the convergence of the solution.

Table 6 shows the results from the implemented variable kinematic models. They are obtained modeling the cylinder at $0 \leq y < L/2$ with lower-order elements (in particular, linear, quadratic, third- and fourth-

order TE elements are used), whereas eleventh-order elements are used at $L/2 \leq y \leq L$. These models are addressed as TE1/11, TE2/11, TE3/11 and TE4/11 models, respectively. Finally, Fig. 17 shows the deformed configuration of the loaded cross-section of the cylinder. In this figure, the variable kinematic models are compared to the eleventh-order TE model. The following considerations arise:

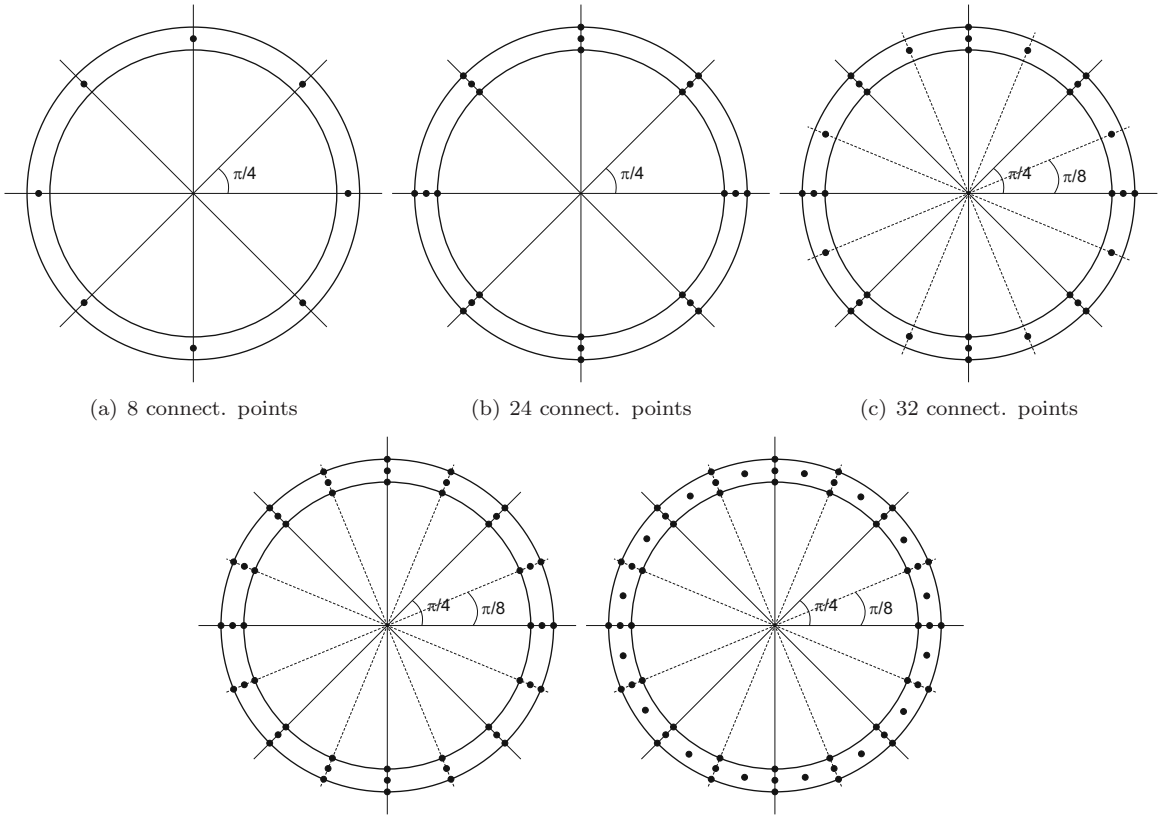

(a) 8 connect. points (b) 24 connect. points (c) 32 connect. points

(d) 48 connect. points (e) 64 connect. points

Figure 16: Location of the connection points on the interface cross-section of the cylinder

	$-u_z$ $[mm]$	DOFs
$TE1/11$	6.12	7533
$TE2/11$	6.15	7812
$TE3/11$	6.18	8184
$TE4/11$	6.20	8649
$TE11$	6.23	14274
SHELL	6.62	60000

Table 6: Vertical displacement of the top loaded point, u_z, and number of unknowns of the variable kinematic models. Pinched cylinder

1. Very high expansion orders are needed to correctly detect the displacement field of the thin-walled cylinder subjected to a pinch type loading condition.

2. The eleventh-order TE model provides good results if compared to the solution from the shell elements model. However, the TE11 model might not be efficient it terms of computational costs, since higher-order elements are also used where cross-sectional displacements are not significant.

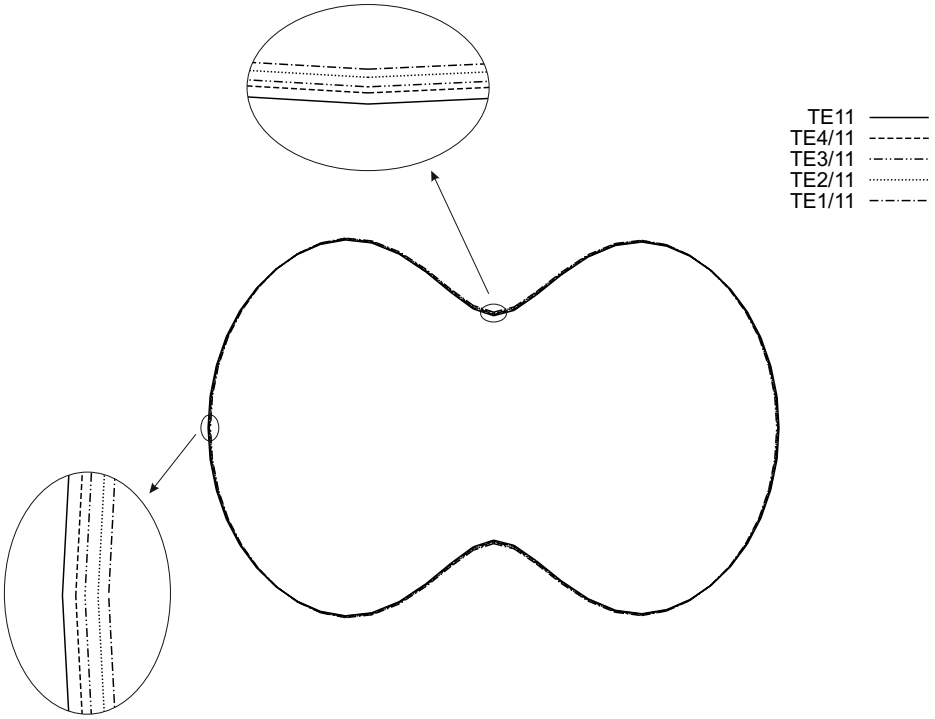

Figure 17: Deformed tip cross-section of the cylinder. Variable kinematic models versus TE11 model

3. Variable kinematic models can be used and high-order elements can be employed in the portion of the structure in which low-order theories would yield inaccurate results, i.e. where the stress field is quasi-three-dimensional.

4. The method of the Lagrange multipliers in conjunction with the CUF make available a reliable formulation to deal with variable kinematic models.

4.4 Bridge-like Section

A clamped-clamped bridge-like beam was analysed next. The geometry was taken from [32]. Figure 18 shows the geometric characteristics of the considered structure and Table 7 presents the dimensions of the beam. The Young's modulus, E, was equal to 210 GPa, whereas the Poisson's ratio, ν was 0.3. 40 B4 elements

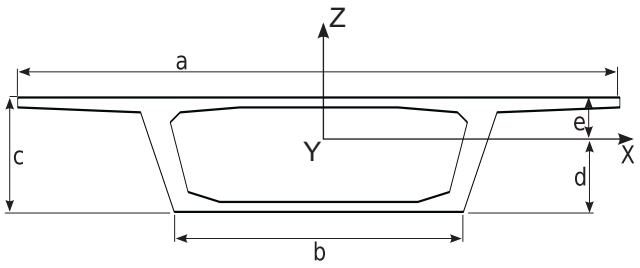

Figure 18: Bridge-like cross-section

with the same length were used in the axial discretization. An MSC/NASTRAN® solid model was used for comparison purposes and it was taken from [23], where the mechanical behavior of the present bridge-like

Dimension	$[m]$
a	15.200
b	7.300
c	3.450
d	2.155
e	1.295
L	100

Table 7: Bridge-like cross-section dimensions

structure was investigated through single-order 1D CUF models. In this work, the torsional analysis of the bridge-like beam was carried by means of variable kinematic models. A uniform distributed linear load, P_L, was applied to the top surface edges of the cross-section, as shown in Fig. 19. P_L is equal to 10^5 N/m.

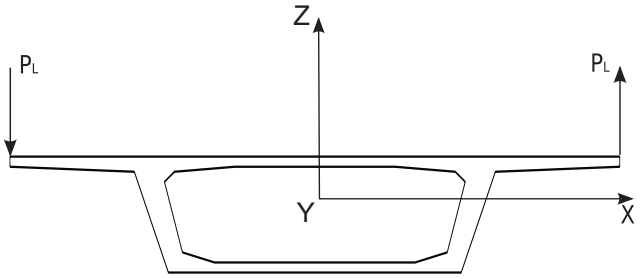

Figure 19: Loading condition of the bridge-like structure

The maximum vertical displacements at $y = L/2$ are given in Table 8. The results from both single and variable kinematic higher-order models as well as classical beam theories are given. The last row shows the values obtained with MSC/NASTRAN®. The location on the cross-section of each of the maximum displacements is reported in the last two columns. The variable kinematic CUF models were obtained according to Fig. 20 and 64 connection points were used on each interface cross-section. The placement and the number of the connection points were chosen on the basis of a convergence study. The placement of the connection points on the interface cross-sections is shown in Fig. 21.

Variable kinematic models are referred to as $TE\alpha/\beta$, where α is the expansion order of the 1D elements used to model the lower-order domains, whereas β is the expansion order of the higher-order area. The three-dimensional deformed configuration of the structure is shown in Fig. 22 and it was obtained through the $TE2/4$ model. Figure 23 shows the deformation of the middle-span cross-section for different beam models.

Model	DOFs	$u\ [mm]$	x	z
		u_x		
EBBM	363	0	-	-
TBM	603	0	-	-
$TE1$	1089	0.267	$-b/2$	$-d$
$TE1/2$	1926	0.418	$-b/2$	$-d$
$TE2$	2178	0.556	$-b/2$	$-d$
$TE1/3$	3018	-0.551	$-a/2$	e
$TE2/3$	3306	-0.707	$-a/2$	e
$TE3$	3630	-0.857	$-a/2$	e
$TE1/4$	4383	-0.582	$-a/2$	e
$TE2/4$	4671	-0.727	$-a/2$	e
$TE3/4$	5055	-0.875	$-a/2$	e
$TE4$	5445	-0.895	$-a/2$	e
$TE2/5$	6309	-0.795	$-a/2$	e
$TE4/5$	7173	-0.971	$-a/2$	e
$TE5$	7623	-1.002	$-a/2$	e
SOLID [23]	351228	-1.100	$-a/2$	0.994
		u_z		
EBBM	363	0	-	-
TBM	603	0	-	-
$TE1$	1089	-0.944	$-a/2$	e
$TE1/2$	1926	-1.738	$-a/2$	e
$TE2$	2178	-2.414	$-a/2$	e
$TE1/3$	3018	-2.168	$-a/2$	e
$TE2/3$	3306	-2.796	$-a/2$	e
$TE3$	3630	-3.144	$-a/2$	e
$TE1/4$	4383	-2.399	$-a/2$	e
$TE2/4$	4671	-2.989	$-a/2$	e
$TE3/4$	5055	-3.334	$-a/2$	e
$TE4$	5445	-3.501	$-a/2$	e
$TE2/5$	6309	-3.353	$-a/2$	e
$TE4/5$	7173	-3.875	$-a/2$	e
$TE5$	7623	-4.028	$-a/2$	e
SOLID [23]	351228	-5.000	$-a/2$	e

Table 8: Value and location of the maximum displacements at $y = L/2$ for different beam theories and comparison with solid elements. Bridge-like section

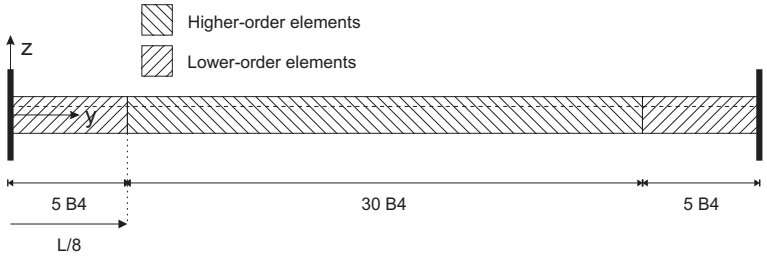

Figure 20: Variable kinematic models of the bridge-like structure

Vectorial shear stress distributions over the cross-section at $y = L/4$ are shown in Fig. 24 for $TE1$, $TE1/2$, $TE1/4$ and $TE4$ models. It should be noted that the variable kinematic models allow for the enhancement of the prediction capabilities of the present formulation in terms of both displacement and stress fields by modelling the areas of interest with higher-order elements. Another example is given in Fig. 25, where shear

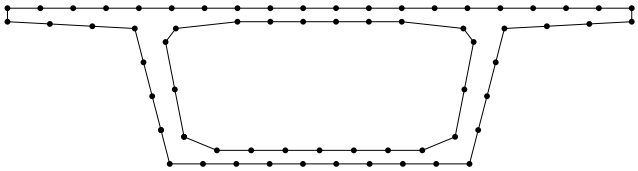

Figure 21: Location of the connection points on the interface cross-sections of the bridge-like structure

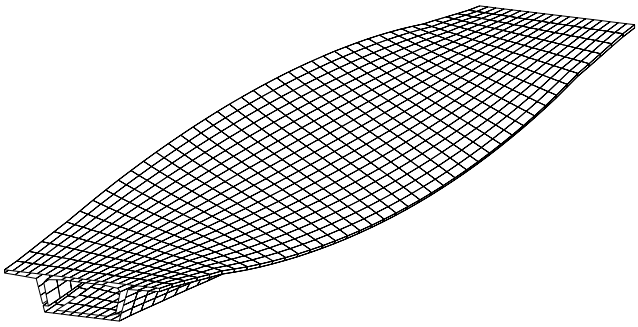

Figure 22: Deformed bridge-like beam, $TE2/4$ model

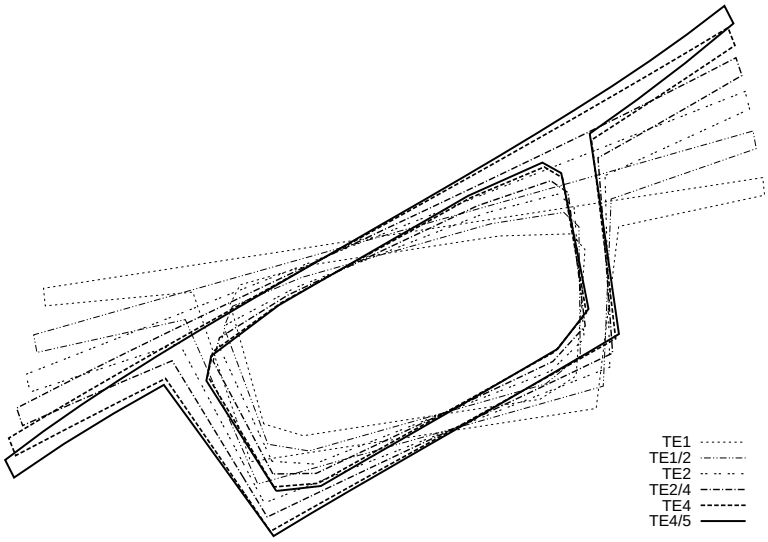

Figure 23: Deformation of bridge-like cross-section beam at $y = L/2$ for different structural models

stress distributions in terms of magnitude are shown for the $TE2/4$, $TE2/5$ and SOLID models. On the other hand, the regions in the neighbourhood of the interface cross-sections between two different order elements can be affected by stress inaccuracies. For example, Fig. 26 shows the Von Mises stress distribution above the cross-section at $y = L/8$ for the single-order $TE4$ model and the variable kinematic $TE2/4$ model. The following comments can be made:

1. The use of refined theories appears to be mandatory to provide significant improvements in the prediction of the torsional structural behavior by means of beam modeling.

2. Variable kinematic models can be used to refine regions of interest also when torsional analysis are considered. However, the convenience in terms of computational saving is not as evident as in the cases

of thin-walled structures undergoing localized loads.

3. Inaccuracies of the stress fields could exist in the close proximity of the interface cross-sections. This phenomenon is well known to be the major drawback of most global/local approaches and it is discussed in several works, such as [13, 33, 34].

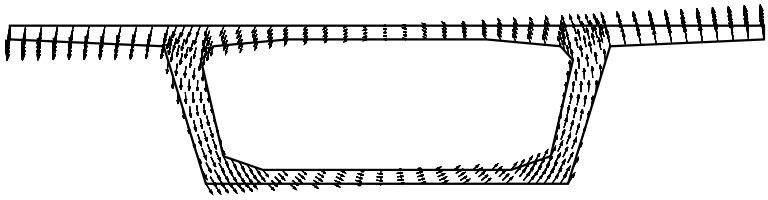

(a) $TE1$

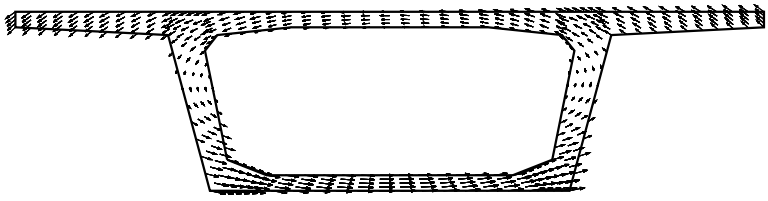

(b) $TE1/2$

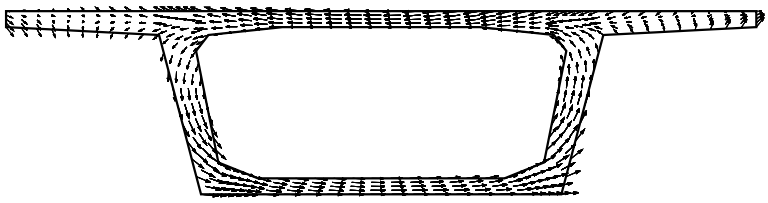

(c) $TE1/4$

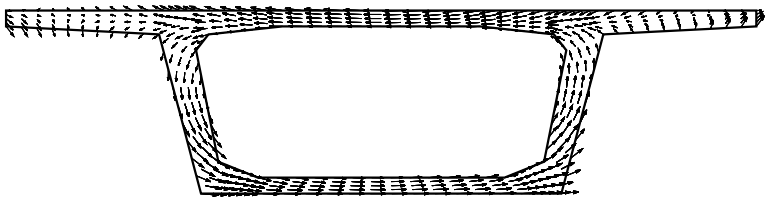

(d) $TE4$

Figure 24: Vectorial shear stress distribution, $\sigma_{xy} + \sigma_{zy}$, at $y = L/4$ for different beam theories

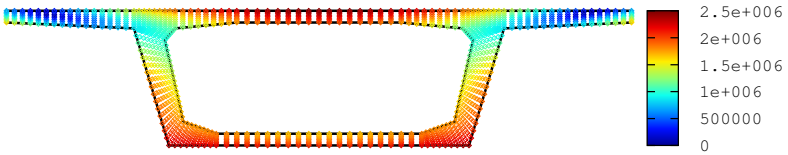

(a) $TE2/4$

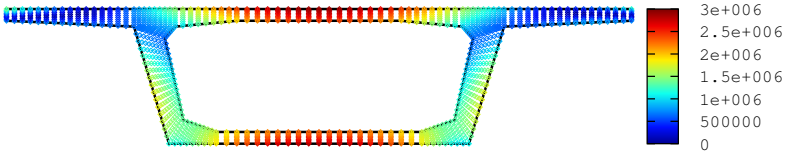

(b) $TE2/5$

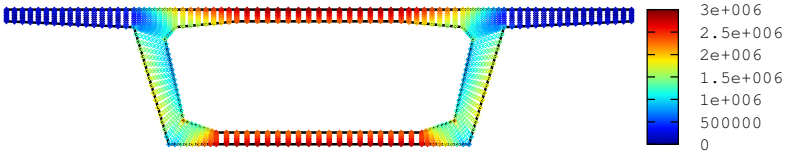

(c) SOLID

Figure 25: Comparison of the shear stress field (Pa) between the variable kinematic beam models and solid elements, $y = L/4$

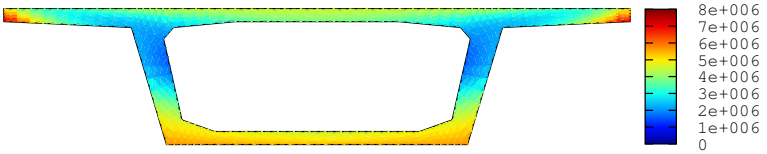

(a) $TE4$

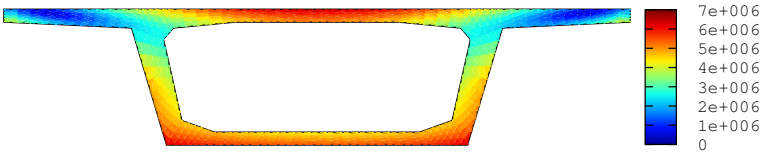

(b) $TE2/4$

Figure 26: Von Mises stress distribution (Pa) at the interface cross-section ($y = L/8$)

5 Conclusions

The extension of the method of Lagrange multipliers to the CUF has been proposed in this paper. The use of the Lagrange multipliers to apply arbitrary boundary conditions on higher-order beam models has been shown. Moreover, a multiple model method was developed and global/local analyses were carried out through variable kinematic models obtained by means of the unified formulation. It is concluded that refined 1D TE models are able to detect complex strain-stress fields, in accordance with more cumbersome 2D and 3D models. Furthermore, kinematic variable models allow a further reduction of computational costs. In fact, higher-order elements are used where a three-dimensional stress-strain field occur, whereas lower-order elements can be used for the subregions of the structure where a refined analysis is not necessary.

References

[1] R. E. Bank. *Adaptive computational methods for partial differential equations.* SIAM, 1983.

[2] B. A. Szabo and I. Babuska. *Finite element analysis.* John Wiley & Sons, 1991.

[3] K. J. Bathe. *Finite element procedure.* Prentice hall, 1996.

[4] J. Fish, L. Pan, V. Belsky, and S. Gomaa. Unstructured multigrid method for shells. *International Journal of Numerical Methods in Engineering*, 39(7):1181–1197, 1996.

[5] N. Möes, J. Dolbow, and T. Belytschko. A finite element method for crack growth without remeshing. *International Journal of Numerical Methods in Engineering*, 46(1):131–150, 1999.

[6] J. Fish. The s-version of the finite element method. *Computers and Structures*, 43(3):539–547, 1992.

[7] J. Fish. Adaptive s-method for linear elastostatics. *Computer Methods in Applied Mechanics and Engineering*, 103:363–396, 1993.

[8] K. W. Shim, D. J. Monaghan, and C. G. Armstrong. Mixed dimensional coupling in finite element stress analysis. *Engineering with Computers*, 18:241–252, 2002.

[9] P. J. Blanco, R. A. Feijoo, and S. A. Urquiza. A variational approach for coupling kinematically incompatible structural models. *Computer Methods in Applied Mechanics and Engineering*, 197:1577–1620, 2002.

[10] K. M. Mao and C. T. Sun. A refined global-local finite element analysis method. *International Journal of Numerical Methods in Engineering*, 32:29–43, 1991.

[11] H. Ben Dhia. Multiscale mechanical problems: the arlequin method. *Comptes Rendus de l'Acadmie des Sciences - Series IIB - Mechanics-Physics-Astronomy*, 326(12):899–904, 1998.

[12] H. Hu, S. Belouettar, M. Potier-Ferry, and E. M. Daya. Multi-scale modelling of sandwich structures using the arlequin method part i: linear modelling. *Finite Elements in Analysis and Design*, 45(1):37–51, 2008.

[13] F. Biscani, G. Giunta, S. Belouettar, E. Carrera, and H. Hu. Variable kinematic beam elements coupled via arlequin method. *Composite Structures*, 93:697–708, 2011. DOI: 10.1016/j.compstruct.2010.08.009.

[14] C. Bernardi, Y. Maday, and A.T. Patera. A new nonconforming approach to domain decomposition: the mortar element method. In H. Brezis and J.L. Lions, editors, *Nonlinear Partial Differential Equations and Their Applications: Collège De France Seminar*, volume XI, pages 13–51. Pitman, 1994.

[15] Q.Z. He, H. Hu, R. Belouettar, G. Giunta, K. Yu, Y. Liu, F. Biscani, E. Carrera, and M. Potier-Ferry. Multi-scale modelling of sandwich structures using hierarchical kinematics. *Composite Structures*, 93:2375–2383, 2011.

[16] K. Kapania and S. Raciti. Recent advances in analysis of laminated beams and plates, part I: Shear effects and buckling. *AIAA Journal*, 27(7):923–935, 1989.

[17] K. Kapania and S. Raciti. Recent advances in analysis of laminated beams and plates, part II: Vibrations and wave propagation. *AIAA Journal*, 27(7):935–946, 1989.

[18] D. H. Hodges. A review of composite rotor blade modeling. *AIAA Journal*, 28(3):561–565, 1990.

[19] S. N. Jung, V. V. Nagaraj, and I Chopra. Assessment of composite rotor modeling techniques. *Journal of the American Helicopter Society*, 44(3):188–205, 1999.

[20] E. Carrera, G. Giunta, and M. Petrolo. *Beam Structures: Classical and Advanced Theories*. John Wiley & Sons, 2011. DOI: 10.1002/9781119978565.

[21] E. Carrera and M. Petrolo. Refined beam elements with only displacement variables and plate/shell capabilities. *Meccanica*, 47(3):537–556, 2012. DOI: 10.1007/s11012-011-9466-5.

[22] E. Carrera, G. Giunta, P. Nali, and M. Petrolo. Refined beam elements with arbitrary cross-section geometries. *Computers and Structures*, 88(5–6):283–293, 2010. DOI: 10.1016/j.compstruc.2009.11.002.

[23] E. Carrera, M. Petrolo, and E. Zappino. Performance of cuf approach to analyze the structural behavior of slender bodies. *Journal of Structural Engineering*, 138(2):285–297, 2012. DOI: 10.1061/(ASCE)ST.1943-541X.0000402.

[24] E. Carrera, M. Petrolo, and P. Nali. Unified formulation applied to free vibrations finite element analysis of beams with arbitrary section. *Shock and Vibrations*, 18(3):485–502, 2011. DOI: 10.3233/SAV-2010-0528.

[25] E. Carrera, M. Petrolo, and A. Varello. Advanced beam formulations for free vibration analysis of conventional and joined wings. *Journal of Aerospace Engineering*, 25(2):282–293, 2012. DOI: 10.1061/(ASCE)AS.1943-5525.0000130.

[26] E. Carrera and M. Petrolo. On the effectiveness of higher-order terms in refined beam theories. *Journal of Applied Mechanics*, 78(3), 2011. DOI: 10.1115/1.4002207.

[27] O. C. Zienkiewicz and R. L. Taylor. *The Finite Element Method for Solid and Structural Mechanics*. Butterworth-Heinemann, Washington, 6th edition, 2005.

[28] S. W. Tsai. *Composites Design*. Dayton, Think Composites, 4th edition, 1988.

[29] J. N. Reddy. *Mechanics of laminated composite plates and shells. Theory and Analysis*. CRC Press, 2nd edition, 2004.

[30] R. Courant. *Differential and Integral Calculus*. Interscience Publishers, 1937.

[31] G. Strang. *Calculus*. Welles-Cambridge Press, 1991.

[32] F. Gruttmann and W. Wagner. Shear correction factors in timoshenko's beam theory for arbitrary shaped cross-sections. *Computational Mechanics*, 27:199–207, 2001.

[33] N. Osawa, H. Hashimoto, J. Sawamura, T. Nakai, and S. Suzuki. Study on shellsolid coupling fe analysis for fatigue assessment of ship structure. *Marine Structures*, 20:143–163, 2007.

[34] J.E. Schiermeier, R. Kansakar, D. Mong, J.B. Ransom, M.A. Aminpour, and W.J. Stroud. p-version interface elements in global/local analysis. *International Journal For Numerical Methods In Engineering*, 53:181–206, 2002.